Thermal Processes of Volatile RuO_2 in Nanocrystalline Al_2O_3 Matrixes Involving $\gamma \rightarrow \alpha$ Phase Transformation

L. Ji,[†,‡] J. Lin,[‡] and H. C. Zeng*[,†]

Department of Chemical and Environmental Engineering, Faculty of Engineering, and Department of Physics, Faculty of Science, National University of Singapore, 10 Kent Ridge Crescent, Singapore 119260

Received December 29, 2000. Revised Manuscript Received April 17, 2001

Thermal processes of the volatile compound RuO_2 in Al_2O_3 matrixes involving phase transformation have been investigated. In this model system, the secondary phase, rutile RuO_2, can be formed and preserved in Al_2O_3 matrixes throughout a wide temperature range (400−1000 °C) due to the nanocrystalline Al_2O_3 that turns on or off matrix reactions with the surrounding RuO_2. At 300−400 °C, nanocrystallites (2 nm) of γ-Al_2O_3 are formed in the presence of ruthenium. Single-phase RuO_2 is formed from its precursor compound at 400 °C, while the intermediate species of Ru^0 and $RuO_2 \cdot xH_2O$ are detected at lower temperatures. The imbedded ruthenium shows a catalytic effect on the early formation of nanocrystalline γ-Al_2O_3 matrix, and the resultant high-surface-area matrix in turn allows the ruthenium to be fully oxidized to RuO_2 in air. The γ-Al_2O_3 matrix is converted to α-phase at ca. 1000 °C. This transformation is promoted by the nanosized RuO_2. A lowering of 60 °C in the transformation temperature has been observed with the presence of only 0.5 wt % of ruthenium. During the phase transformation, an abrupt matrix-crystallite growth takes place (from 2−3 to 40 nm), which leads to a denser α-Al_2O_3 matrix, protecting RuO_2 from thermal evaporation at high temperature. The utilization of other important thermal processes observed (such as evaporation−condensation) in fabrication of nanostructured materials is also addressed.

Introduction

In recent years, synthesis and characterization of nanostructured materials have attracted great attention, owing to many new properties generated for these materials.[1−8] Nanocomposites, which have a great application potential in many highly technological areas, such as quantum confinement, heterojunctions, and nanostructured catalysts, are a combination of two or more phases comprising different chemical compositions or structures, and one of the chemical/structural phases must be in nanometric scale.[9−14]

In preparation of inorganic nanocomposite materials such as metal oxides, for example, a number of fundamental issues should be addressed: (i) formation process and precursor chemistry of nanocrystallite oxide matrix; (ii) formation process of secondary oxide phase, which includes also confinement chemistry of both precursor compound and the resulting oxide; (iii) possible phase transformations or solid-state processes (such as crystallite growth, evaporation, or condensation of volatile oxide components upon heating or cooling); and (iv) the extra complexity that will be added if there are chemical reactions between the confined oxide(s) and calcination atmospheres. Although the actual processes in a synthesis are complicated, the processes sometimes reveal their own clues. The evaporation process, for example, can reflect indirectly the intrinsic structure (such as surface area and crystallite size) of the solid matrix. In this regard, a volatile secondary phase itself can also serve as a probe compound to understand the synthetic preparation in general. Unlike the common perception, "bad" processes such as evaporation of a volatile component can sometimes become desirable. The evaporation may be utilized to generate a concentration gradient

* To whom correspondence should be addressed.Tel: +65 874 2896. Fax: +65 779 1936. E-mail: chezhc@nus.edu.sg.
† Department of Chemical and Environmental Engineering
‡ Department of Physics

(1) Elder, S. H.; Cot, F. M.; Su, Y.; Heald, S. M.; Tyryshkin, A. M.; Bowman, M. K.; Gao, Y.; Joly, A. G.; Balmer, M. L.; Kolwaite, Ana C.; Magrini, K. A.; Blake, D. M. *J. Am. Chem. Soc.* **2000**, *122*, 5138.
(2) Zhang, Q.; Remsen, E. E.; Wooley, K. L. *J. Am. Chem. Soc.* **2000**, *122*, 3642.
(3) Wang, Z. L. *J. Phys. Chem. B* **2000**, *104*, 1153 and the references therein.
(4) Moller, K.; Bein, T. *Chem. Mater.* **1998**, *10*, 2950; and the references therein.
(5) Ying, J. Y.; Mehnert, C. P.; Wong, M. S. *Angew. Chem., Int. Ed.* **1999**, *38*, 56 and the references therein.
(6) Corriu, R. J. P. *Angew. Chem., Int. Ed.* **2000**, *39*, 1376 and the references therein.
(7) Bradley, J. S.; Tesche, B.; Busser, W.; Maase, M.; Reetz, M. T. *J. Am. Chem. Soc.* **2000**, *122*, 4631.
(8) Richards, R.; Li, W.; Decker, S.; Davidson, C.; Koper, O.; Zaikovski, V.; Volodin, A.; Rieker, T.; Klabunde, K. J. *J. Am. Chem. Soc.* **2000**, *122*, 4921.
(9) Gangopadhyay, R.; De, A. *Chem. Mater.* **2000**, *12*, 608.
(10) Ishida, H.; Campbell, S.; Blackwell, J. *Chem. Mater.* **2000**, *12*, 1260.
(11) Yamashita, Y.; Yoshida, K.; Kakihana, M.; Uchida, S.; Sato, T. *Chem. Mater.* **1999**, *11*, 61.
(12) Zarbin, A. J. G.; Vargas, M. D.; Alves, O. L. *J. Mater. Chem.* **1999**, *9*, 519.
(13) Sankar, J.; Sham, T. K.; Puddephatt, R. J. *J. Mater. Chem.* **1999**, *9*, 2439.
(14) Shabtai, K.; Rubinstein, I.; Cohen, S. R.; Cohen, H. *J. Am. Chem. Soc.* **2000**, *122*, 4959.

10.1021/cm001420q CCC: $20.00
Published on Web 06/22/2001

starting from the center of a matrix if one wishes to prepare functional gradient materials.[15,16]

Most metal oxide formations involve metal reactions with ambient oxygen. Due to different metal reactivities, underoxidized, undesired species are often formed in the oxide composites prepared by conventional methods, especially for the secondary phase that is imbedded in matrix oxides and lacks oxygen accessibility. The term "nanoconfinement" used in our work means that the secondary phase is confined within a nanocrystalline oxide matrix with controlled crystallite size and surface area. In this sense, matrix reactions with the surrounding gases (or other chemicals) can be switched on or off. For instance, fuller interactions of an imbedded secondary phase with the ambient atmosphere during a thermal treatment are expected when crystallites of matrix oxide are small and the specific surface area of the matrix is high.

We will demonstrate the above confinement effect through investigation on thermal processes of sol−gel derived RuO_2–Al_2O_3 nanocomposites with Ru wt % = 0.5−2.0. The system is selected because it is a suitable material combination for an investigation of the above complex issues altogether, in addition to the normal formation of RuO_2–Al_2O_3. For example, the matrix material Al_2O_3 formed from aluminum hydroxides and oxyhydroxides evolutes through a series of hydrate phases (γ, δ, θ, etc.) to a thermodynamically stable phase (corundum α-Al_2O_3) at high temperatures.[17] The secondary phase RuO_2, on the other hand, is unstable at elevated temperatures and becomes the gaseous species RuO_3 and RuO_4 due to the reactions with oxygen. These interconnected physicochemical processes during the synthesis will cause changes in chemical composition, structure, and thus the ultimate performance of the composites.

Apart from the above fundamental interests, the imbedded component RuO_2 has been found in use in a wide variety of important applications such as active catalysts for Fischer−Tropsch conversion and combustion,[18] charge storage (hydrous form),[19] RuO_2-based anode materials,[20−22] and solid conducting electrodes in microelectronic devices.[23] As for the matrix material, Al_2O_3 has been widely used in many technologically important areas such as refractory ceramic, catalyst, catalyst support and adsorbent. Alumina in the γ-and α-phases is also one of the main constituents of rocket exhaust formed by rocket motors.[24] Therefore, the present investigation is also aimed at a better understanding on the formation of RuO_2-containing nanocomposites in general.[11−13]

Experimental Section

Sample Preparation. Xerogel precursors for RuO_2–Al_2O_3 nanocomposites were prepared by combining 10 mmol of aluminum tri-*sec*-butoxide (Al(O-*s*-Bu)$_3$, or ASB, ACROS, 97%), 150 mmol of 2-propanol (*i*-PrOH, Fisher Scientific, >99.9%), and 5 mmol of the chelating agent 2,4-pentanedione (acetylacetone, $C_5H_8O_2$ or acacH, Merck, >99.5%) under nitrogen atmosphere. The mixed solution was agitated for 30 min and a solution of Ru-red ($Cl_6H_{42}N_{14}O_2Ru_3 \cdot 4H_2O$ or $[(NH_3)_5Ru^{III}O(NH_3)_2Ru^{IV}(NH_3)_2ORu^{III}(NH_3)_5]Cl_6 \cdot 4H_2O$, Fluka, >95%) dissolved in 120 or 60 mmol of deionized water was then added dropwise with continuous stirring for another 30 min. The mole ratio of water to alkoxide (ASB) was kept at 12 (the sample series A; 120 mmol of water) and 6 (the sample series B; 60 mmol of water), while the metal content of ruthenium in gel was defined by the weight ratio of Ru wt % = 0.5, 1.0, and 2.0. The samples are thus called A-0.5, A-1.0, and A-2.0 and B-0.5, B-1.0, and B-2.0, respectively. Blank alumina gel samples were also prepared for comparison in a similar way, except no Ru-red was dissolved in the deionized water.

Gelations of the above-prepared solutions took place within 5 days. The resulting wet transparent gels were aged at room temperature for another 5 days, which was followed by a drying in an electric oven at 60 °C for 5 days. The resultant xerogels were calcined in static air at 300, 400, 600, 800, and 1000 °C, respectively, for 2 h with a heating rate of 5 °C min^{-1}.

Characterization Techniques. *FTIR Measurement.* Chemical bonding information on metal-oxygen, hydroxyl, and other functional groups was obtained with Fourier transform infrared spectroscopy (FTIR, Perkin-Elmer Model 2000) using the potassium bromide (KBr) pellet technique. The FTIR spectrum background was corrected using a freshly prepared pure KBr pellet. Each spectrum was collected after 32 scans at a resolution of 4 cm^{-1}.

XRD Measurement. Crystallographic information on the samples was investigated by powder X-ray diffraction (XRD). Diffraction patterns of intensity vs 2θ were recorded with a Shimadzu XRD-6000 X-ray diffractometer using Cu Kα radiation (λ = 1.5418 Å). A continuous scan mode was used to collect 2θ data from 10° to 80° with a 0.02 sampling pitch and a 4° min^{-1} scan rate. X-ray tube voltage and current were set at 40 kV and 30 mA, respectively. The average crystallite sizes of the samples were estimated using the Debye−Scherrer formula from the full width-at-half-maximum (fwhm) of some intense peaks.[25]

TEM Measurement. Investigation with high-resolution transmission electron microscopy (TEM) was carried out on a Philips FEG CM300 with an electron kinetic energy of 300 kV. The specimens for TEM imaging were prepared by suspending about 1 mg samples in deionized water. A small container filled with the aqueous suspension was placed in an ultrasonic water bath and sonicated for 30 min. A drop of this well-dispersed suspension was placed on a carbon-coated 300-mesh copper grid, followed by drying the sample under ambient conditions before it was attached to the sample holder of the microscope.

DTA/TGA Measurement. The study with differential thermal analysis (DTA, Perkin-Elmer 7 Series UNIX V4.0) was carried out to understand the thermal behaviors of Ru-red and as-prepared gels. About 20 mg of gel sample was heated at a rate of 10 °C min^{-1} with a flow of air at 22.7 mL min^{-1} over 40−1400 °C, using a standard powder sample of alumina as a reference. Thermogravimetric analysis (TGA, Shimadzu TGA-50) was conducted in order to understand thermal decomposition processes of Ru-red and formation of RuO_2. In each run of TGA, about 20−35 mg of Ru-red sample was heated at 10

(15) Cherradi, N.; Kawasaki, A.; Gasik, M. *Composites Eng.* **1994**, *4*, 883.
(16) Zhu, J. C.; Yin, Z. D.; Lai, Z. H. *J. Mater. Sci.* **1996**, *31*, 5829.
(17) Leonard, A. J.; Van Cauwelaert, F.; Fripiat, J. J. *J. Phys. Chem.* **1967**, *71*, 6.
(18) Over, H.; Kim, Y. D.; Seitsonen, A. P.; Wendt, S.; Lundgren, E.; Schmid, M.; Varga, P.; Morgante, A.; Ertl, G. *Science* **2000**, *287*, 1474.
(19) (a) Zheng, J. P.; Cygan, P. J.; Jow, T. R. *J. Electrochem. Soc.* **1995**, *142*, 2699. (b) McKeown, D. A.; Hagans, P. L.; Carette, L. P. L.; Russell, A. E.; Swider, K. E.; Rolison, D. R. *J. Phys. Chem. B* **1999**, *103*, 4852.
(20) Arikawa, T.; Takasu, Y.; Murakami, Y.; Asakura, K.; Iwasawa, Y. *J. Phys. Chem. B* **1998**, *102*, 3736.
(21) Colomer, M. T.; Jurado, J. R. *Chem. Mater.* **2000**, *12*, 923.
(22) Kristof, J.; Daolio, S.; De Battisti, A.; Piccirillo, C.; Mihaly, J.; Hovath, E. *Langmuir* **1999**, *15*, 1498.
(23) Iembo, A.; Fuso, F.; Arimondo, E.; Ciofi, C.; Pennelli, G.; Curro, G. M.; Neri, F.; Allegrini, M. *J. Mater. Res.* **1997**, *12*, 1433.
(24) Laredo, D.; McCrorie, J. D., III.; Vaughn, J. K.; Netzer, D. W. *J. Propulsion Power* **1994**, *10*, 410.
(25) Cheetham, A. K.; Day, P. *Solid-State Chemistry: Techniques*; Clarendon Press: Oxford, 1987; p 79.

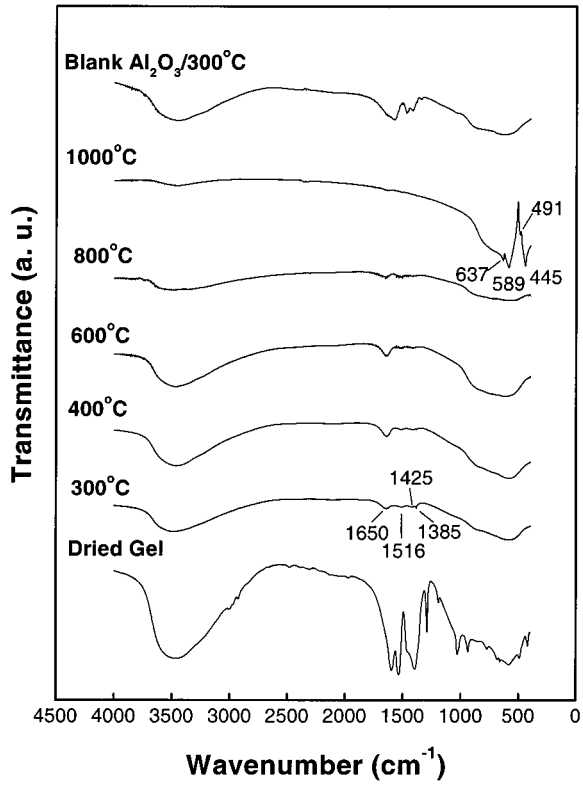

Figure 1. FTIR spectra of as-prepared A-2.0 sample (dried gel) and its related samples after heating at different temperatures for 2 h in static air, noting that the blank alumina gel heated at 300 °C (2 h) is also shown for comparison.

°C min^{-1} in pure nitrogen, pure oxygen, purified air, and N_2O (N_2O 30% balanced with He) respectively at a flow rate of 60 mL min^{-1}.

BET Measurement. Adsorption isotherms of nitrogen at −195.8 °C on all calcined samples were measured at various partial pressures in a Quantachrome NOVA-2000 apparatus.[26,27] Specific surface areas (S_{BET}) were determined with the Brunauer−Emmett−Teller (BET) method (six points in the region of $0.05 < P/P^o < 0.30$; nitrogen molecular cross-sectional area = 16.2 Å^2). Before the measurements, the samples were degassed for 3 h at 250−350 °C in an outgassing station of the adsorption apparatus.

XPS Measurement. The XPS investigation was conducted on a VG ESCALAB-MKII spectrometer using Mg Kα X-ray source (1253.6 eV, 120 W) at the constant analyzer pass energy of 20.0 eV. All binding energies (BE; C 1s, O 1s, Al 2p, and Ru $3d_{5/2,3/2}$) were referenced to the Al 2p peak of Al_2O_3 (BE = 73.7 eV; note that aluminum is a predominant matrix element and Al 2p data in γ-Al_2O_3 and α-Al_2O_3 are almost identical)[28] as an internal standard. Curve-fitting was carried out using a nonlinear (Shirley type) least-squares fitting program with a sum function of 80% Gaussian and 20% Lorentzian. The spin−orbital splitting of the Ru $3d_{5/2,3/2}$ doublet was constrained to be 4.17 eV. [29,30]

Results

Chemical Species in Gel Matrixes. Figure 1 shows a series of FTIR spectra for sample A-2.0 upon heating. The as-prepared xerogel shows typical IR absorptions of aluminum acetylacetonate linkages over the wavenumber range 1900−900 cm^{-1} [ν(C−O) and ν(C−C), etc.],[31] which indicates that the chelating agent acetylacetone is still confined in the gel matrix.[26] The broad absorptions below 900 cm^{-1} correspond to the Al−O−Al network formed after hydrolysis. The three low-intensity bands that appear at 3000−2900 cm^{-1} are assigned to the stretching vibration of C−H bonds in the acac groups.[32,33] These bands disappear when the gel is stabilized upon heating. A broad, intense band at 3473 cm^{-1} corresponds to the residual O−H groups of the synthesized products occluded within the fresh gel.[27,34]

The majority of the organics were dismissed when the sample was calcined at 300 °C. In the 1000−400 cm^{-1} region, the typical stretching vibrations of the Al−O bonds emerge.[35,36] However, without ruthenium, only a small portion of the organics (acac) can be decomposed at 300 °C, as the acac−Al absorption features are still retained (see blank alumina gel, Figure 1). We therefore believe that the presence of ruthenium ions is responsible for the early decomposition of the organics in the gel matrixes. The IR spectra change little at higher calcination temperatures; note that the fingerprint feature of γ-Al_2O_3 has appeared at a temperature as low as 300 °C.[26,35] At 1000 °C, four sharp peaks appear at 445−637 cm^{-1}, originating from the α-Al_2O_3 phase.[26,35] During the calcinations, water (bending mode, 1650 cm^{-1}),[36] nitrate (from decomposed Ru-red, 1385 cm^{-1}, 300 °C),[34] and carbonate ions (1516 and 1425 cm^{-1})[34,37,38] are formed in almost all the calcined samples, which is in agreement with the reported observations in the literature on the easy adsorptions of H_2O and CO_2 on RuO_2 or support surfaces.[29,39]

The strong bands at ca. 3470 cm^{-1} of the FTIR spectra are assigned to hydroxyl O−H stretching.[27,36] It is expected that these hydroxyl groups are originally H-bonded to the retained anions, since the hydroxyl bands are shifted toward higher wavenumbers when the anions are depleted from the samples upon heating (600−800 °C, Figure 1). At 1000 °C, the gel matrix is practically dehydroxylated and the high wavenumber O−H band is diminished, as there are no interactions between the hydroxyls and the retained anions.

The included ruthenium dioxide (RuO_2; observed by both XRD and TEM) in the gel matrixes has a rutile

(26) Ji, L.; Lin, J.; Tan, K. L.; Zeng, H. C. *Chem. Mater.* **2000**, *12*, 931.
(27) Ji, L.; Lin, J.; Zeng, H. C. *J. Phys. Chem. B* **2000**, *104*, 1783.
(28) Moulder, J. F.; Stickle, W. F.; Sobol, P. E.; Bomben, K. D. *Handbook of X-ray photoelectron spectroscopy: a reference book of standard spectra for identification and interpretation of XPS data;* Chastain, J., Ed.; Perkin-Elmer Corp.: Minneapolis, MN, 1992.
(29) Kim, K. S.; Winograd, N. *J. Catal.* **1974**, *35*, 66.
(30) Chan, H. Y. H.; Takoudis, C. G.; Weaver, M. J. *J. Catal.* **1997**, *172*, 336.
(31) (a) Guertin, D. L.; Wiberley, S. E.; Bauer, W. H.; Goldenson, J. *J. Phys. Chem.* **1956**, *60*, 1018. (b) Nakamoto, K. *Infrared Spectra of Inorganic and Coordination Compounds*; John Wiley and Sons: New York, 1962; p 216; Nakamoto, K. *Infrared and Raman Spectra of Inorganic and Coordination Compounds*; John Wiley and Sons: New York, 1986; p 259. (c) Leaustic, A.; Babonneau, F.; Livage, J. *Chem. Mater.* **1989**, *1*, 240.
(32) Zeng, H. C.; Shi, S. *J. Non-Cryst. Solids* **1995**, *185*, 31.
(33) Chuang, C. C.; Wu, W. C.; Huang, M. C.; Huang, I. C.; Lin, J. L. *J. Catal.* **1999**, *185*, 423.
(34) Chellam, U.; Xu, Z. P.; Zeng, H. C. *Chem. Mater.* **2000**, *12*, 650.
(35) Gadsden, J. A. *Infrared spectra of minerals and related inorganic compounds*; Butterworths: London, 1975; p 43.
(36) Chisem, I. C.; Jones, W. *J. Mater. Chem.* **1994**, *4*, 1737.
(37) Ji, W.; Chen, Y.; Shen, S.; Li, S.; Wang, H. *Appl. Surf. Sci.* **1996**, *99*, 151.
(38) Hsieh, B. R.; Ettedgui, E.; Gao, Y. *Synth. Met.* **1996**, *78*, 269.
(39) Bruce, L. A.; Hoang, M.; Hughes, A. E.; Turney, T. W. *J. Catal.* 1998, *178*, 84.

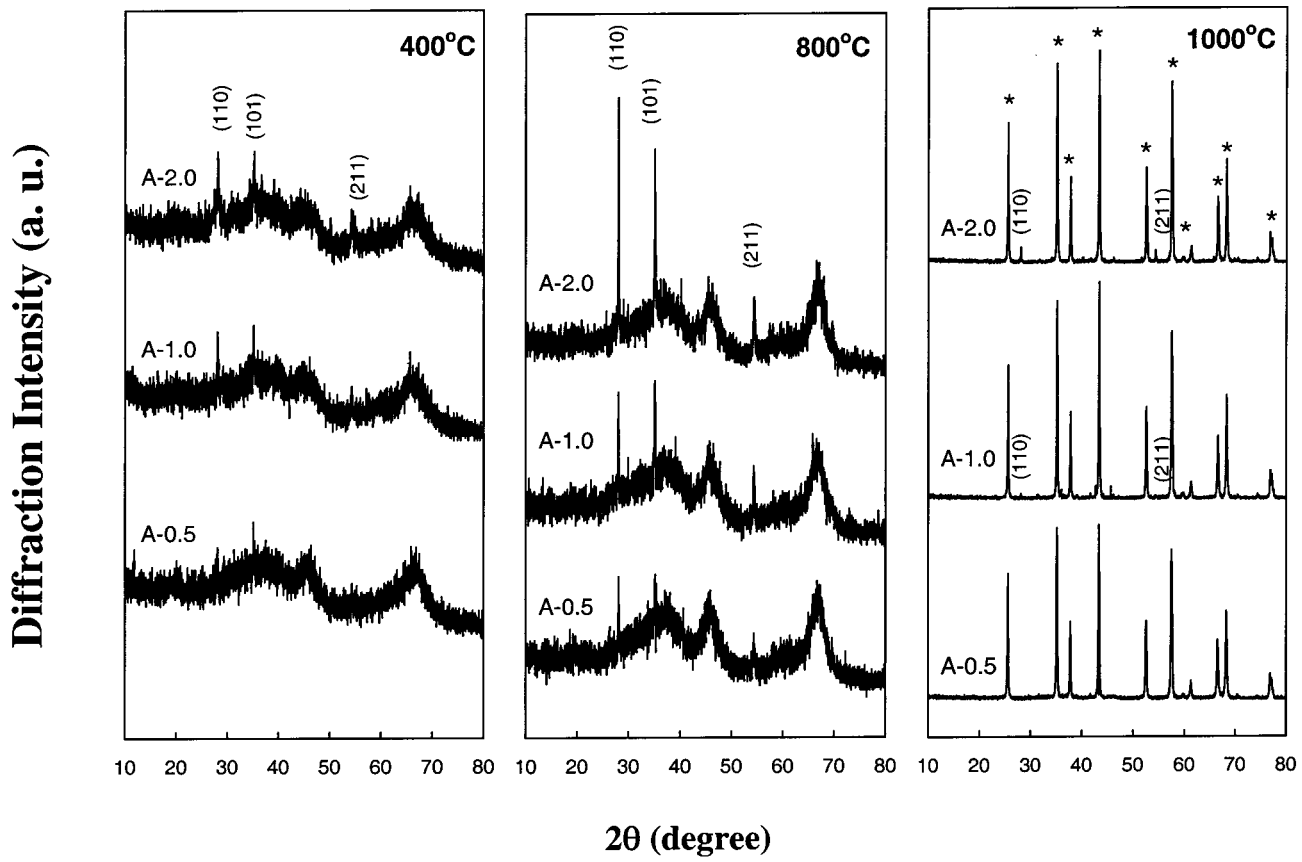

Figure 2. XRD patterns of A-series samples (with different Ru loadings) after heated in static air at 400 °C (a), 800 °C (b), and 1000 °C (c) for 2 h.

structure and it is the most thermally stable species in the family of Ru oxides. Being a conductive oxide, nonetheless, the ruthenium dioxide cannot be positively identified by FTIR.[30,40] Therefore, our FTIR spectra for A-0.5, A-1.0, and A-2.0 are almost identical (Ru = 0.5−2.0 wt %) because RuO_2 is IR-inactive. The water concentration used in the preparation has indeed exceeded the required level and gives no effect on the chemical composition of the gels, since the FTIR spectra of sample series A and B are also identical.

Formation of Nanocomposites. The above FTIR chemical investigation has also indicated that the formation of γ-Al_2O_3 from the xerogels starts at 300 °C and the transformation of the γ-phase to α-Al_2O_3 starts at 1000 °C. The formation of the nanocomposites, alumina and ruthenium dioxide (IR inactive), is reported in Figure 2 for the samples of the A-series. The secondary phase, rutile RuO_2,[41] starts to form at 400 °C and is proportional to the initial ruthenium content in the xerogels (400 °C, Figure 2), although the major diffraction peaks belong to the γ-Al_2O_3 phase.[41] The diffraction patterns for both γ-Al_2O_3 and rutile RuO_2 become more resolved at 800 °C, which indicates a continuous growth of crystallites upon the calcinations (800 °C, Figure 2). No diffraction of metallic Ru phase (Ru^0) can be detected, although it had been observed in Ru/Al_2O_3 catalyst prepared by a sol−gel method.[42] At 1000 °C, transformation of γ-Al_2O_3 into the α-phase occurs (1000 °C, Figure 2), while the diffraction of RuO_2 has been reduced. Nonetheless, RuO_2 is still present in A-1.0 and A-2.0, although it becomes undetectable in A-0.5. Finally, it should be mentioned that the samples in the B-series give essentially the same diffraction patterns as those of Figure 2. Once again, the water content in the initial gel preparation does not cause an extra effect on the nanocomposite formation.

Table 1. Calculated Crystallite Sizes of RuO_2–Al_2O_3 Nanocomposites in the Sample Series A

calcination temp (°C)	crystallite size of Al_2O_3 (nm) [a]			crystallite size of RuO_2 (nm) [b]		
	A-0.5	A-1.0	A-2.0	A-0.5	A-1.0	A-2.0
400	1.6	1.6	1.6	9.8	8.5	12.8
600	1.9	1.7	1.8	9.8	26.8	28.7
800	2.7	2.3	2.7	11.7	33.3	53.9
1000	43.4	37.2	38.9	-	45.5	51.8

[a] Mean crystallite size of Al_2O_3 is estimated from fwhms of the (211) peak ($2\theta = 66.8°$) of γ-Al_2O_3 or the (104) peak ($2\theta = 35.2°$) of α-Al_2O_3. [b] Mean crystallite size of RuO_2 is estimated from fwhms of (110) peak ($2\theta = 28.1°$).

The crystallite sizes of the matrix Al_2O_3 and the included RuO_2 crystallites were determined by the fwhms of the XRD peaks and are summarized in Table 1.[41] Apparently, high metal content and high-temperature calcination favor the formation of larger crystallites. In this connection, high-resolution transmission electron micrographs also show a high dispersity of RuO_2 in alumina matrixes. As expected, the crystallite

(40) Bewick, A.; Gutierrez, C.; Larramona, G. *J. Electroanal. Chem.* **1992**, *332*, 155.

(41) Powder Diffraction Files: γ-Al_2O_3 (#01−1308, #10−0425), RuO_2 (#40−1290), Ru (#06−0663); Joint Committee on Powder Diffraction Standards, Swarthmore, PA, 1995.

(42) Lopez, T.; Herrera, L.; Mendez-Vivar, J.; Bosch, P.; Gomez, R.; Gonzalez, R. D. *J. Non-Cryst. Solids* **1992**, *147&148*, 773.

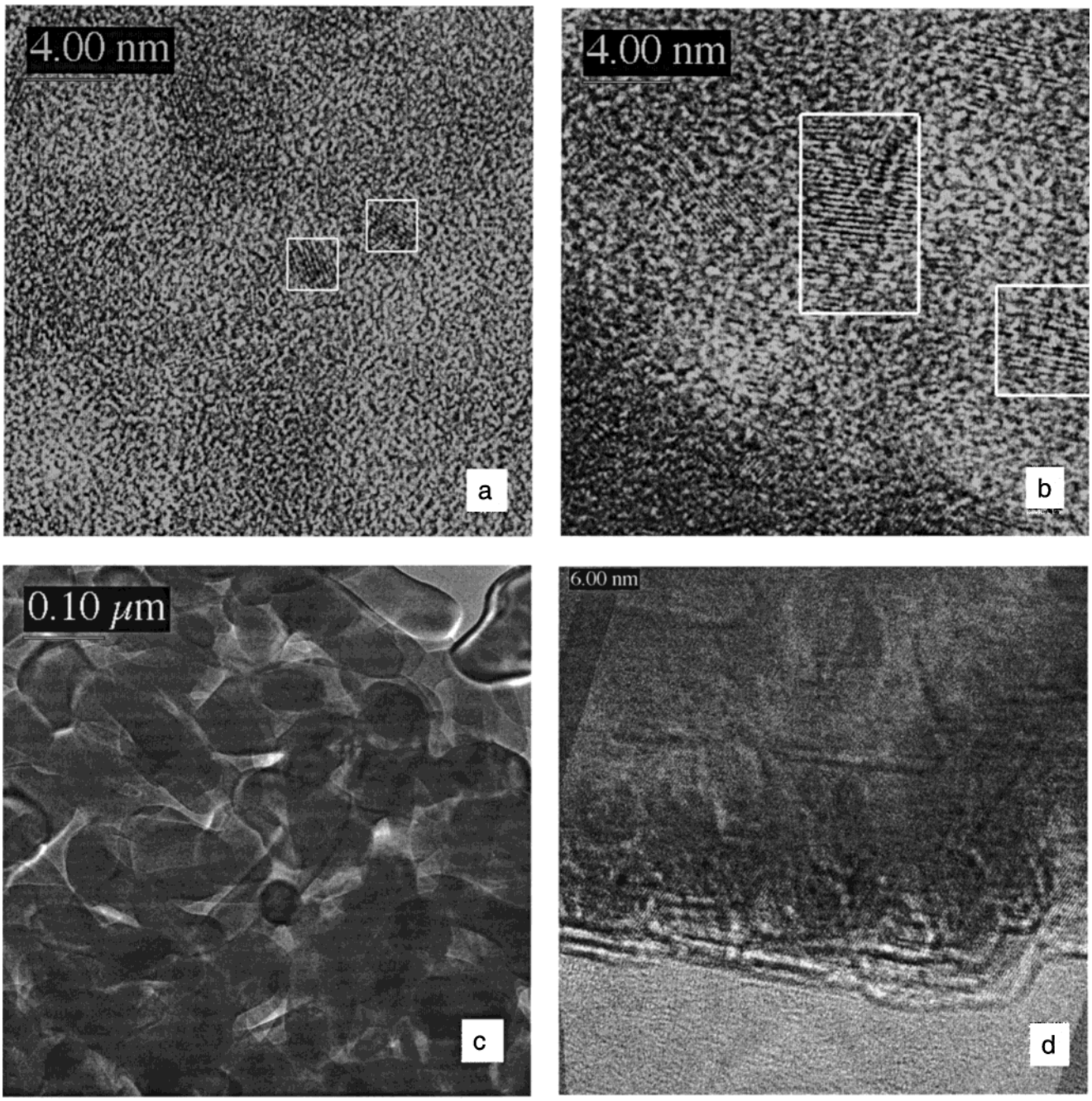

Figure 3. High-resolution TEM micrographs of A-0.5 sample after heating in static air at 400 °C (a and b) for 2 h and A-2.0 sample after heated in static air at 1000 °C (c and d) for 2 h.

size increases with increasing temperature. In Figure 3a,b, even in the low-metal-content sample A-0.5 (heated at 400 °C), both γ-Al_2O_3 and RuO_2 crystallites can be observed simultaneously. In particular, the interplane distances d_{311} of the γ-Al_2O_3 nanoparticles ($d_{311} = 0.23$ nm, framed in Figure 3a) and d_{110} of the RuO_2 phase ($d_{110} = 0.33$ nm, framed in Figure 3b, together with d_{311} of γ-Al_2O_3) can be located. The crystallite sizes observed by TEM here are in good agreement with the XRD data in Table 1.[41] When the temperature reaches 1000 °C, high-density α-Al_2O_3 phase is formed and the matrix structure is shown in Figure 3c,d for sample A-2.0. The α-Al_2O_3 particles (Figure 3c) are polycrystalline, since their sizes are in the range of 100−150 nm, about 2−3 times greater than those determined by XRD (~40 nm, Table 1). The interplane distances d_{113} (0.209 nm) and d_{104} (0.255 nm) of the α-phase have been clearly seen with higher magnifications. As an example, both the hexagonal symmetry of the (001) surface (i.e., (0001) plane) and the interplane distance of d_{113} (0.209 nm) of α-Al_2O_3 can be clearly observed in Figure 3d.

Thermal Evolution Processes. DTA scans for the blank alumina xerogel and pure Ru-red solid samples are displayed in Figure 4 (upper diagram). For the blank alumina heated in air atmosphere, the endothermic band at 182 °C is attributed to depletions of trapped water and PrOH that were produced as byproducts of gelation reactions. The large exothermic band centered at 430 °C is assigned to the decomposition/oxidation of residual carbon and other organic functional groups (Figure 1).[26] This exothermic band in fact starts much earlier at ca. 300 °C, which corresponds also to the

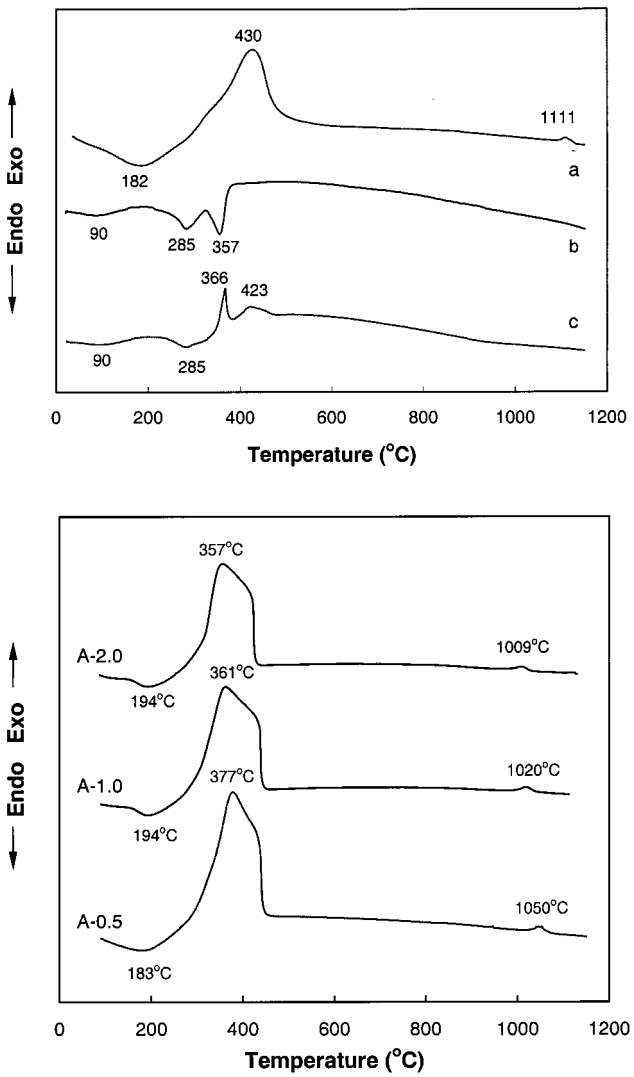

Figure 4. Upper diagram: DTA scans for (a) as-prepared blank alumina gel heated in air, (b) Ru-red compound heated in N_2, and (c) Ru-red compound heated in air. Lower diagram: DTA scans for A-series of samples heated in air.

formation of γ-Al_2O_3 from the amorphous gel. Another low-intensity exothermic peak is observed at 1111 °C, which can be assigned unambiguously to the transformation of γ-Al_2O_3 to the α-phase (confirmed also with XRD study, not shown here).

Solid Ru-red compound shows different thermal decomposition behaviors in air and nitrogen atmospheres. In Figure 4 (upper diagram), two small endothermic dips at around 90 °C can be assigned to the detachment of water molecules in the compound. Two broad endothermic peaks at 285 °C can be attributed to the removal of external anions Cl^- (×6) and a sharp endothermic peak at 357 °C (in N_2 scan) to the removal of 14 NH_3 ligands and 2 bridging O atoms bonded to Ru^{3+} or Ru^{4+} ions. These DTA assignments are also confirmed with our TGA result (Ru-red in N_2) that shows a clear weight loss for each thermal event; i.e., the observed weight losses are close to the theoretical values of −8.4%, −24.8%, and −31.5% for these steps. It is interesting to note that, on the basis of the TGA result, Ru-red compound is finally decomposed to metallic Ru^0 in nitrogen atmosphere but to the RuO_2 in air or pure oxygen. In oxidative atmospheres (air or O_2), the decomposition of Ru-red and oxidation of evolving NH_3 with O_2 occurs simultaneously, giving a net exothermic peak at 366 °C. The broad exothermic band at 423 °C can be assigned to the oxidative formation of RuO_2 (from Ru^0), which will be further discussed shortly.

Table 2. Specific Surface Areas (S_{BET}) of Different Nanocomposite Samples

calcination temp (°C)	specific surface area ($m^2\,g^{-1}$) A-0.5	B-0.5	A-2.0	blank alumina
300	430	425	415	580
400	466	460	479	475
600	299	287	301	318
800	239	242	235	234
1000	9	11	10	55

Table 3. Binding Energy (eV) of Ruthenium Oxides and Alumina System[28−30,39]

compd	Ru $3d_{5/2}$	O 1s
Ru	280.0−280.3	
RuO_2	280.7−281.0	529.4−530.0 (lattice)
		531.5−531.7 (adsorbed)
RuO_3	282.5−282.6	530.7
RuO_4	283.3	
$RuO_2{\cdot}xH_2O$	281.4−281.8	529.3 (oxide)
		530.5 (H_2O)
$RuOCO_3$		530.5 (CO_3^{2-})
γ-Al_2O_3		530.9
α-Al_2O_3		531.8

DTA curves for the samples of the A-series are also shown in Figure 4 (lower diagram). At low metal content (A-0.5), an endothermic peak at 183 °C is observed, which corresponds to the depletion of the trapped water and solvent/byproducts, as assigned before for the blank alumina gel (Figure 4). This band is shifted to a higher temperature (194 °C) when the metal content is increased (A-1.0 and A-2.0). The detachment of Cl^- anions (285 °C, Figure 4) is not observable, while the temperature of decomposition of Ru-red and oxidation of evolved NH_3 is metal-content dependent. The temperature lowering from 377 to 357 °C indicates clearly the effect of matrix confinement (i.e., decrease in difficulty) on the related chemical reactions. The combustion of residual carbons and organic groups of $Al(O\text{-}s\text{-}Bu)_{3-n}(acac)_n$,[26] which peaks at 430 °C in the blank alumina gel, takes place now in a more abrupt manner, as shown in the sudden drop of the band. Since this temperature range is also for the formation of RuO_2, the combustion reactions may be catalyzed in the presence of RuO_2, noting the temperature cutoff is moved to lower temperature side when the metal content is increased. Transformation of γ-Al_2O_3 to α-Al_2O_3 can be observed in a small exothermic peak at 1009−1050 °C. Without ruthenium, the $\gamma \rightarrow \alpha$ transition occurs at 1111 °C (Figure 4, upper diagram). Even with the ruthenium content as low as 0.5 wt %, a temperature lowering of ca. 60 °C has been achieved. This early $\gamma \rightarrow \alpha$ transformation can be attributed to the insertion of the nanocrystalline RuO_2 in the alumina matrixes, which blocks γ-Al_2O_3 crystallites from growing when heated.

Surface Analysis of Nanocomposites. Specific surface areas (S_{BET}) of the calcined xerogels are listed in Table 2. The S_{BET} values show a similar trend for all the samples, i.e., the ruthenium concentration and H_2O: ASB give no obvious effects on the final S_{BET}. Neverthe-

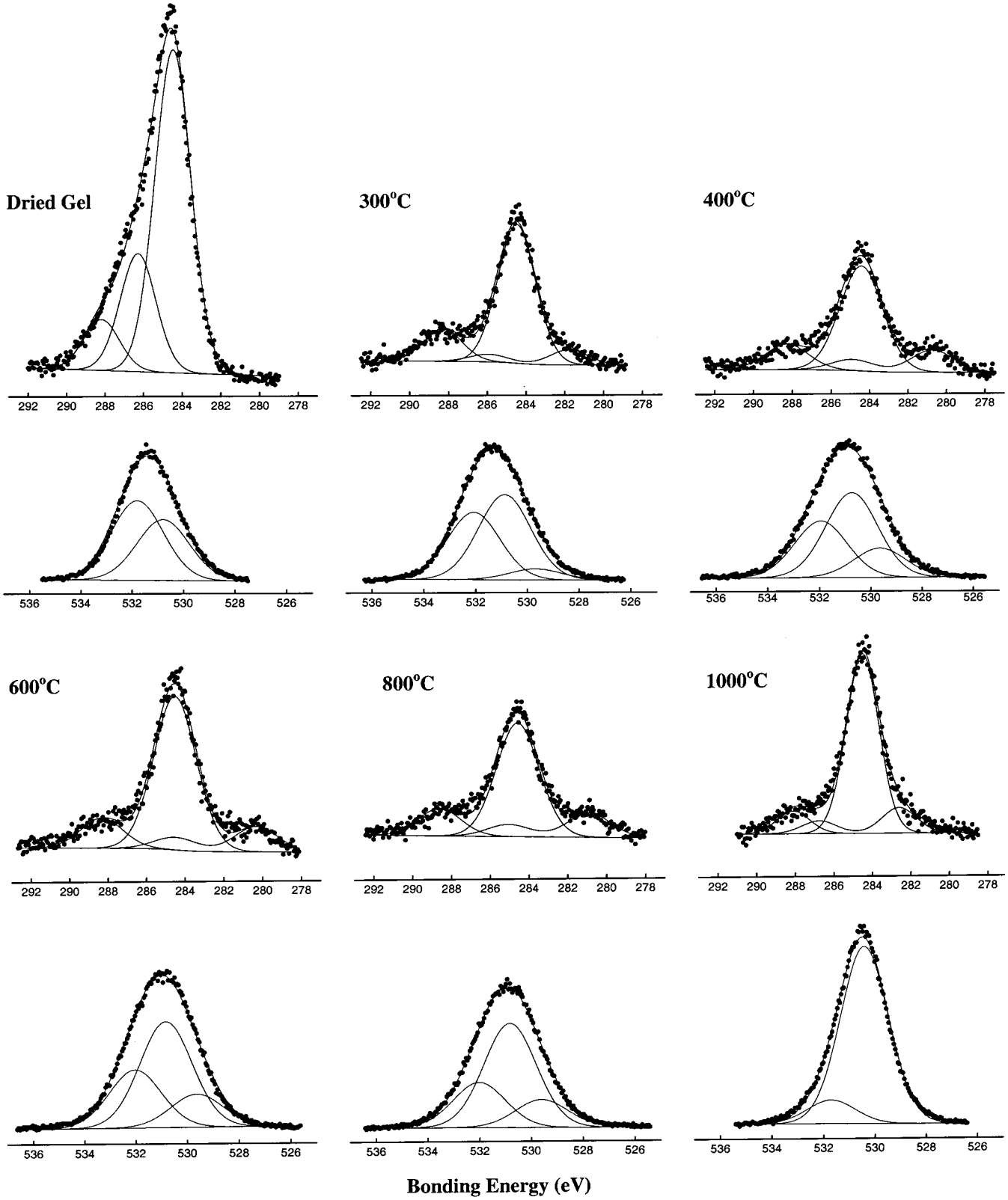

Figure 5. XPS spectra of Ru $3d_{5/2,3/2}$ and C 1s (together in top curves, 292−278 eV) and O 1s (bottom curves, 536−526 eV) levels of as-prepared A-2.0 sample (dried gel) and its related samples after heated at different temperatures for 2 h in static air.

less, unlike the blank alumina gel, the S_{BET} of which maximizes at 300 °C, the ruthenium-containing gels give a S_{BET} peak at 400 °C, which corresponds to the decomposition of Ru-red, oxidation of NH_3, and formation of RuO_2 (DTA results, Figure 4). When heated at higher temperatures, crystallite growth becomes important (TEM results, Figure 3 and Table 1) for alumina and a significant decrease in S_{BET} is observed at 1000 °C when the $\gamma \rightarrow \alpha$ transformation takes place.

The XPS analysis of different Ru oxides has been well documented in the literature, and Table 3 summarizes some published results for reference.[29,30,39] In Figure 5, some representative curve-fitted Ru $3d_{5/2,3/2}$ doublet and O 1s XPS spectra of the A-2.0 sample are displayed as

a function of calcination temperature. For the as-prepared A-2.0 sample, no Ru $3d_{5/2,3/2}$ photoelectrons are observed on the surface before calcination. The peaks at 288.2, 286.3, and 284.5 eV are assigned to the C═O double bond (in acac),[29] C−O single bond (trapped ROH, R is alkyl groups) and surface contaminated carbon.[28] The corresponding O 1s XPS spectrum consists of two peaks at 531.8 and 530.8 eV that are assigned to oxygen atoms in C═O (and also O−C═O)[28,38] and Al−O, respectively.[28]

After calcination at 300 °C, Ru $3d_{5/2}$ at 281.8 eV is associated with the formation of hydrated RuO_2 ($RuO_2 \cdot xH_2O$), and the two C 1s peaks at 288.3 and 284.5 eV are attributed to CO_3^{2-} and surface contaminated carbon. In the O 1s region, three peaks are deconvoluted. The O1s peak located at 532.1 eV can be attributed to the carbonate group and that at 530.9 eV is mostly likely due to a mixture of Al−O (in γ-phase) and H_2O. The O 1s from hydrated RuO_2 can be observed at 529.7 eV.[29,39]

Calcination of the sample at 400 °C shifts the Ru $3d_{5/2}$ peak maximum from 281.8 to 280.7 eV. This shift can be attributed to dehydration of $RuO_2 \cdot xH_2O$ and thus the formation of RuO_2 (Table 3).[29,30,39] The O 1s peak intensity at 531.9 eV decreases, which makes the 529.7 eV peak (lattice oxygen in RuO_2) more distinctive.[29,30] Upon further increasing calcination temperature to 800 °C, little changes can be found.

A noticeable shift of the Ru $3d_{5/2}$ peak to 282.6 eV (RuO_3, Table 3)[29] is observed upon the calcination at 1000 °C, along with the two C 1s peaks at 288.1 and 284.5 eV. Instead of RuO_2, which is found in the bulk phase by XRD (Figure 2), RuO_3 (Table 3) is formed/adsorbed on the α-Al_2O_3 matrix surface. A new O 1s peak at 530.4 eV is attributable to oxygen in surface RuO_3 or a surface complex of Ru−O−Al. The α-Al_2O_3 matrix is largely covered by the RuO_3 surface species, as only a small O 1s peak at 531.9 eV for the matrix oxygen is observed (α-Al_2O_3, Table 3).

Discussion

Preparation of Alumina Matrixes. When an ASB molecule is fully hydrolyzed, three water molecules are required; i.e., the reaction stoichiometric ratio of H_2O:alkoxide (ASB) is 3:1. When the H_2O:alkoxide ratio is in excess of that required for the stoichiometry, the extent of hydrolysis is observed as highly branched polymeric products and an increase in cross-linking. Accordingly, physicochemical properties of single metal oxides and mixed metal oxides can be altered by varying the H_2O:alkoxide ratio in the sol−gel syntheses.[43−48] For example, it has been found that the variation in surface area can be as high as 273 $m^2\ g^{-1}$ if H_2O:ASB ratios are 6 and 15 (625 $m^2\ g^{-1}$ vs. 352 $m^2\ g^{-1}$), respectively.[45] In our experiments, excess water was used [H_2O:ASB ratio = 12 (A series) and 6 (B series)] in order to hydrolyze ASB fully. Although the H_2O:ASB ratios used in the A- and B-series are quite different, there is no obvious difference in the S_{BET} data (Table 2), which indeed indicates that the water effect on the final oxide texture/morphology has been minimized. To minimize the effect of water on the sol−gel process and thus particle sizes of alumina matrixes, in this work, acacH was used as the chelating agent to slow the hydrolysis rate. It should be mentioned that in our experiments, the mole ratio of ASB:acacH was equal to 2:1.[49] Any increase in acacH content in the synthesis would cause a significant increase in gelation time. In fact, when the initial ASB:acacH ratio was equal to 1:1, no gelation occurred under our experimental conditions.

In this work, transparent gels rather than colloidal precipitates had been obtained when hydrolysis was performed in the presence of acacH. Moreover, the use of the chelating agents is also aimed to improve the sintering property.[50] Strong chelating agents are considered to remain partially in the gel matrixes, even after elimination of physically adsorbed water upon drying (e.g., Figure 1, dried gel) and before decomposition upon calcination (e.g., < 300 °C, Figure 1). Through the processes of condensation and drying, the chelating agents might prevent the growth of the alumina particles by forming a protective coating on the surface during the initial stage of calcination.[49,50] This may also explain why alumina crystallite growth was modest and the S_{BET} values remain more than 200 $m^2\ g^{-1}$ even after calcination at 800 °C.

Bulk and Surface Ruthenium Oxides. The source ruthenium compound Ru-red has the chemical structure $[(NH_3)_5Ru^{III}O(NH_3)_2Ru^{IV}(NH_3)_2ORu^{III}(NH_3)_5]Cl_6 \cdot 4H_2O$. As reported in our DTA/TGA studies, Ru-red decomposes first to Ru^0 (weight loss ~64%) in the inert atmosphere of nitrogen, but to RuO_2 (weight loss ~53%) in air or oxygen. To confirm the Ru^0 formation, which results from the presence of intramolecular reducing reagents (Cl− and NH_3), decomposition of the solid Ru-red with the TGA method was further conducted in N_2O atmosphere (N_2O has only a moderate oxidation strength). As expected, the weight loss analysis indicates a total decomposition down to metallic ruthenium (Ru^0; the theoretical weight loss from Ru-red, −64.7%), and then a subsequent oxidation up to RuO_2 (theoretical weight gain from Ru^0, +11.2%) in the N_2O atmosphere. Although the two thermal processes cannot be distinguished in air, we believe metallic ruthenium is also formed before RuO_2. Therefore, the secondary phase RuO_2 in the present nanocomposite system is started from Ru^0:

$$Ru + O_2(g) \rightarrow RuO_2(s) \quad (1)$$

Nonetheless, in our 300 °C-heated A-2.0 sample (Figure 5), hydrated RuO_2 ($RuO_2 \cdot xH_2O$ or $RuO_{2-y}(OH)_y$ with $0 < y < 2$) is formed:[19]

$$RuO_2(s) + yH^+ + ye^- \leftrightarrow RuO_{2-y}(OH)_y(s) \quad (0 < y < 2) \quad (2)$$

The compounds $RuO_{2-y}(OH)_y$ have been detected in our

(43) Zhan, Z.; Zeng, H. C. *J. Mater. Chem.* **1999**, *9*, 2647.
(44) Yamane, M.; Aso, S.; Okano, S.; Sakaino, T. *J. Mater. Sci.* **1979**, *14*, 607.
(45) Balakrishnan, K.; Gonzalez, R. D. *J. Catal.* **1993**, *144*, 395.
(46) Zou, W. Q.; Gonzalez, R. D. *J. Catal.* **1995**, *152*, 291.
(47) Lopez, T. *React. Kinet. Catal. Lett.* **1992**, *47*, 21.
(48) Lopez, T.; Asomoza, M.; Gomez, R. *J. Non-Cryst. Solids.* **1992**, *147&148*, 769.
(49) Nass, R.; Schmidt, H. *J. Non-Cryst. Solids* **1990**, *121*, 329.
(50) Maeda, K.; Mizukami, F.; Niwa, S.; Toba, M.; Watanabe, M.; Masuda, K. *J. Chem. Soc. Faraday. Trans.* **1992**, *88*, 97.

XPS study (Figure 5), although they are undetectable by the XRD method (because the compounds are amorphous or poorly crystalline[19b]). The formation of $RuO_{2-y}(OH)_y$ indicates that the Ru^0 is not fully oxidized to Ru^{4+} (as in eq 1) by O_2 at 300 °C; note that the bulk phase RuO_2 is formed only at 400 °C (XRD result, Figure 2). When RuO_2 is heated in oxygen, the following two reversible reactions have been reported to occur:[29,51]

$$RuO_2(s) + {}^1/_2O_2(g) \leftrightarrow RuO_3(g) \quad (3)$$

$$RuO_2(s) + O_2(g) \leftrightarrow RuO_4(g) \quad (4)$$

The predominant species in the gas phase at temperatures greater than 1000 °C is RuO_3 and at lower temperatures (800 °C) is RuO_4.[29,51] These results suggest that RuO_4 and/or RuO_3 may be present on the surface of RuO_2 or the surfaces of alumina matrixes, as most of the high bonding energy species may be formed when the sample is being cooled.[23,29,52,53] The RuO_2 surface is often covered with oxygen adsorbed upon it, but the surface oxygen may act as a barrier against further oxidation. The formation of RuO_3 has been observed on the surface of single-crystal RuO_2, and it has been suggested that RuO_3 plays a significant role in stabilizing the RuO_2 surface.[53] Other investigations have also indicated that RuO_3 is formed in Ru/Al_2O_3 catalyst,[52] RuO_2 thin film,[23] and RuO_2 powder.[29] Nonetheless, adsorbed (or condensed) RuO_4 is not detected (Ru $3d_{5/2}$ at 283.3 eV, Table 3) in our samples due to the decomposition of RuO_4 (the reverse reaction of eq 4) at room temperature.[30]

Since surface RuO_2 can be easily oxidized into gaseous RuO_4 and RuO_3 at high temperatures,[29,51] the evolving RuO_4 and/or RuO_3 are the origin of ruthenium loss during calcinations, which explains why there is no more surface RuO_2 when the samples were calcined at 1000 °C (XPS result, Figure 5). As for the bulk-phase RuO_2, which has been imbedded within the alumina matrixes, the oxidation reactions of eqs 3 and 4 cannot be pursued so easily. This is evidenced in the XRD patterns of A-1.0 and A-2.0 samples even after high-temperature calcinations at 1000 °C (Figure 2). It should be mentioned that this matrix protection is not perfect. In the low metal content sample A-0.5, neither surface nor bulk RuO_2 can be detected after 1000 °C calcinations (Figure 2).

The metallic Ru^0 is vulnerable toward oxidizing to the higher valent oxides RuO_2, RuO_3, or RuO_4. Using different Ru precursors, the Ru^0 phase has been found in the sol−gel prepared catalysts $Ru-Al_2O_3$ by the XRD technique[42] and the supported catalysts Ru/Al_2O_3 (after reductions in various gases) by the XPS method.[52] Compared to the former sol−gel method, which forms Ru^0, RuO_2, and γ-Al_2O_3 simultaneously at 600 °C (samples with $S_{BET} \leq 114$ m^2 g^{-1}),[42] the present method can produce a single-phase RuO_2 in γ-Al_2O_3 matrixes at a temperature as low as 400 °C. This can be attributed to the formation of nanocrystalline matrix material and high surface areas listed in Tables 1 and 2, which allows a full oxidation of imbedded Ru^0 metal with gas-phase oxygen (eq 1).

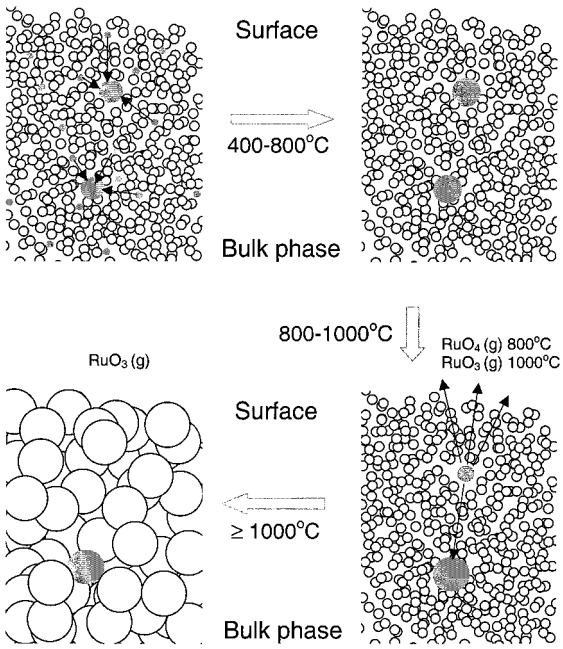

Figure 6. Cross-section views of a proposed mechanism based on the present findings; dark gray particles indicate the confined RuO_2, while the light gray particles (circled) indicate the Al_2O_3 matrix; note that one large RuO_2 is located in the surface region while the other is in the bulk phase. The arrows indicate the diffusion (inside the matrix) or evaporation (to gas phase outside the matrix) directions of the RuO_2 particles.

Crystallite Growth and $\gamma\rightarrow\alpha$ Transformation. In many sol−gel derived material systems, particle size is an important parameter affecting physical properties such as phase transformation. The general observation is that the smaller the particle size, the easier the transformation.[54] Nevertheless, as phase transformation normally occurs at elevated temperatures, the thermally accelerated grain growth is sometimes unavoidable. Regarding the current alumina $\gamma\rightarrow\alpha$ transformation at ca. 1000 °C, we have observed an abrupt crystallite growth of the alumina matrixes from 800 to 1000 °C (Table 1 and Figure 3). Compared to the alumina growth, the crystallite growth of RuO_2 is much smoother over the same temperature range (Table 1), which can be attributed to continued growth upon heating. Since the secondary phase RuO_2 acts as foreign particles, which isolates γ-Al_2O_3 crystallites prior to the phase transition to the α-phase, it is not surprising that the $\gamma\rightarrow\alpha$ transformation has been promoted when the content of ruthenium is increased.

Figure 6 summaries some findings of the present work. As an effect of the thermal treatment, ionic species (Ru^{4+} and O^{2-}) of small ruthenium oxide crystallites could migrate within the alumina matrixes to join larger crystallites at low heating temperatures (i.e., crystallite growth at 400−800 °C, Table 1). At higher temperatures, the evaporation of RuO_2 becomes operational, causing a surface migration of the RuO_2. This is true for the RuO_2 located near the surface region, as any of these surface crystallites will further react with

(51) Bell, W. E.; Tagami, M. *J. Phys. Chem.* **1963**, *67*, 2432.
(52) Nagai, M.; Koizumi, K.; Omi, S. *Catal. Today*. **1997**, *35*, 393.
(53) (a) Atanasoska, L.; O'Grady, W. E.; Atanasoski, R. T.; Pollak, F. H. *Surf. Sci.* **1988**, *202*, 142. (b) Atanasoska, L.; Atanasoski, R. T.; Pollak, F. H. O'Grady, W. E. *Surf. Sci.* **1990**, *230*, 95.
(54) Zhan, Z.; Zeng, H. C. *J. Mater. Res.* **1998**, *13*, 2174 and the references therein.

gaseous oxygen according to eqs 3 and 4 to leave the surface (800−1000 °C). On the basis of a comparison of relative peak intensities of XRD patterns (800 °C versus 1000 °C, Figure 2), it is found that while the ruthenium has been depleted considerably from α-Al_2O_3 matrixes, the crystallite growth of RuO_2 continues (Table 1). This observation, together with our XPS result (Figure 5), in fact confirms that the ruthenium depletion occurs mainly in the surface region (800−1000 °C, Figure 6), while the confined RuO_2 in the inner matrixes can be exempted from reactions eqs 3 and 4 even at a temperature as high as 1000 °C (within a 2 h heating). Nonetheless, in terms of the $\gamma \rightarrow \alpha$ transformation, 1000 °C is a very low temperature for α-Al_2O_3 matrix preparation. It should be mentioned that some of the gaseous species RuO_4 and RuO_3 at 800 and 1000 °C are respectively decomposed/condensed on the surfaces of alumina matrixes when samples are cooled, as discussed for the XPS result (Figure 5). In addition to the homogeneous nanocomposites RuO_2−Al_2O_3 prepared at low temperatures (400−800 °C), functional gradient nanocomposites can also be prepared by utilizing the evaporation and condensation processes (800−1000 °C). As reported in our present study, surface evaporation allows creation of a concentration gradient of RuO_2 crystallites along the radius of the alumina matrixes,[15,16] while the condensation generates an additional shell structure on the external surface of the matrixes;[1,2] note that further selections of surface component and matrix phase are possible. In principle, the growth of the shelled surface oxides can be prevented using a dynamic purging stream of inner gas during the evaporation if they are undesirable.

Conclusions

In summary, we have demonstrated complex thermal processes of RuO_2 encapsulated in nanocrystalline γ-Al_2O_3 matrixes. In particular, low-temperature formation of γ-Al_2O_3 matrixes (at 300−400 °C) with crystallite sizes of 2 nm and specific surface areas of 420−480 m^2 g^{-1} allows us to explore various physicochemical phenomena occurring in this material system upon heating. The secondary component RuO_2 can be formed concurrently with γ-Al_2O_3 matrixes in the single-phase via sequential formations of Ru^0 and hydrous RuO_2 ($RuO_2 \cdot xH_2O$). The imbedded ruthenium shows a catalytic effect on the early formation of nanocrystalline γ-Al_2O_3 matrix, and the resultant high-surface-area matrix in turn allows the ruthenium to be fully oxidized to RuO_2 in air. At ca. 1000 °C, the γ-Al_2O_3 matrixes are transformed into the α-phase, accompanying a significant crystallite growth (from 2−3 to 40 nm). This transformation is promoted by the nanosized RuO_2. A lowering of 60 °C for the transformation temperature has been observed with the presence of only 0.5 wt % of ruthenium. Due to the surface evaporation, loss of RuO_2 from the alumina matrixes has been observed at 800−1000 °C. In this connection, surface RuO_2 and RuO_3 on the γ- and α-Al_2O_3 matrixes are detected, which results from RuO_4 decomposition and RuO_3 condensation upon cooling. Although RuO_2 is unstable at high temperature, our findings allow one to select the Al_2O_3 matrixes with low-temperature γ-phase or high-temperature α-phase while the single-phase RuO_2 remains unaltered.

Acknowledgment. The authors gratefully acknowledge research funding (R-279-000-064-112 and A/C50384) cosupported by the Ministry of Education and the National Science and Technology Board of Singapore. L.J. wishes to thank the National University of Singapore for providing a postgraduate scholarship.

CM001420Q